Dovepress

ORIGINAL RESEARCH

Preparation of Luvangetin Nanoemulsions: Antimicrobial Mechanism and Role in Infected Wound Healing

Yang Chong[1,2], Dong Yu[1,2], Rui Han[3], Yanxu Li[2], Yali Gu[3], Zhaoyu Lu[1,2], Fengsong Nie[1,2], Lingli Wang ⓘ[1], Hengmi Cui[4]

[1]Department of Traditional Chinese Medicine, The Affiliated Hospital of Yangzhou University, Yangzhou University, Yangzhou, Jiangsu, 225000, People's Republic of China; [2]Department of General Surgery, The Affiliated Hospital of Yangzhou University, Yangzhou University, Yangzhou, Jiangsu, 225000, People's Republic of China; [3]Institute of Translational Medicine, Medical College, Yangzhou University, Yangzhou, 225009, People's Republic of China; [4]Institute of Epigenetics and Epigenomics and College of Animal Science and Technology, Yangzhou University, Yangzhou, Jiangsu, 225009, People's Republic of China

Correspondence: Yang Chong, Department of Traditional Chinese Medicine, The Affiliated Hospital of Yangzhou University, Yangzhou University, Yangzhou, Jiangsu, 225000, People's Republic of China, Email 092016@yzu.edu.cn; Hengmi Cui, Institute of Epigenetics and Epigenomics and College of Animal Science and Technology, Yangzhou University, Yangzhou, Jiangsu, 225009, People's Republic of China, Email hmcui@yzu.edu.cn

Purpose: Incorporation of luvangetin in nanoemulsions for antimicrobial and therapeutic use in infected wound healing.

Patients and Methods: Luvangetin nanoemulsions were prepared by high-speed shear method and characterized based on their appearance structure, average droplet size, polydispersity index (PDI), electric potential, storage stability. Optimized formulation of luvangetin nanoemulsion by Box-Behnken design (BBD). The antimicrobial activity and antimicrobial mechanism of luvangetin nanoemulsions against common hospital pathogens, ie, *Staphylococcus aureus (S. aureus)* and *Escherichia coli (E. coli)*, were investigated using luvangetin nanoemulsions. The biosafety of luvangetin nanoemulsion was evaluated through cytotoxicity, apoptosis, and reactive oxygen species (ROS) assay experiments using human normal epidermal cells and endothelial cells. Finally, the effect of luvangetin nanoemulsion on healing of infected wounds was investigated in B6 mice.

Results: Luvangetin nanoemulsion formulation consists of 2.5% sunflower seed oil, 10% emulsifier Span-20 and 7 minutes of shear time, and with good stability. Luvangetin nanoemulsion produces antibacterial activity against *S. aureus* and *E. coli* by disrupting the structure of bacterial cell membranes. Luvangetin nanoemulsion are biologically safe for HaCat and HUVEC. Luvangetin nanoemulsion showed good therapeutic effect on MRSA infected wounds in mice.

Conclusion: For the first time, developed a new formulation called luvangetin nanoemulsion, which exhibited superior antibacterial effects against Gram-positive bacteria. Luvangetin nanoemulsion has a favorable effect in promoting infected wound healing. We have combined luvangetin, which has multiple activities, with nanoemulsions to provide a new topical fungicidal formulation, and have comprehensively evaluated its effectiveness and safety, opening up new possibilities for further applications of luvangetin.

Keywords: luvangetin, nanoemulsion, antimicrobial mechanism, infected wound healing

Introduction

As the body's largest organ, the skin serves as the primary defense against invasion by foreign pathogens. Cutaneous wound healing is a finely balanced biological process comprised of four phases: hemostasis, inflammation, proliferation, and remodeling.[1] Disruption of these regulatory mechanisms at any stage can lead to chronic or non-healing wounds, where persistent inflammation, barrier compromise, impaired oxygenation responses, bacterial infections, age, and disease states can impede the skin's effective wound repair.[2–5] In fact, chronic wounds are frequently accompanied by bacterial infections, which contribute to the formation of chronic wounds.[5,6] Infected wound healing presents a significant challenge in cutaneous wound treatment, imposing severe emotional and financial burdens on patients.[7] Given that bacterial infections are a primary cause of chronic inflammation and delayed wound healing, addressing these

Graphical Abstract
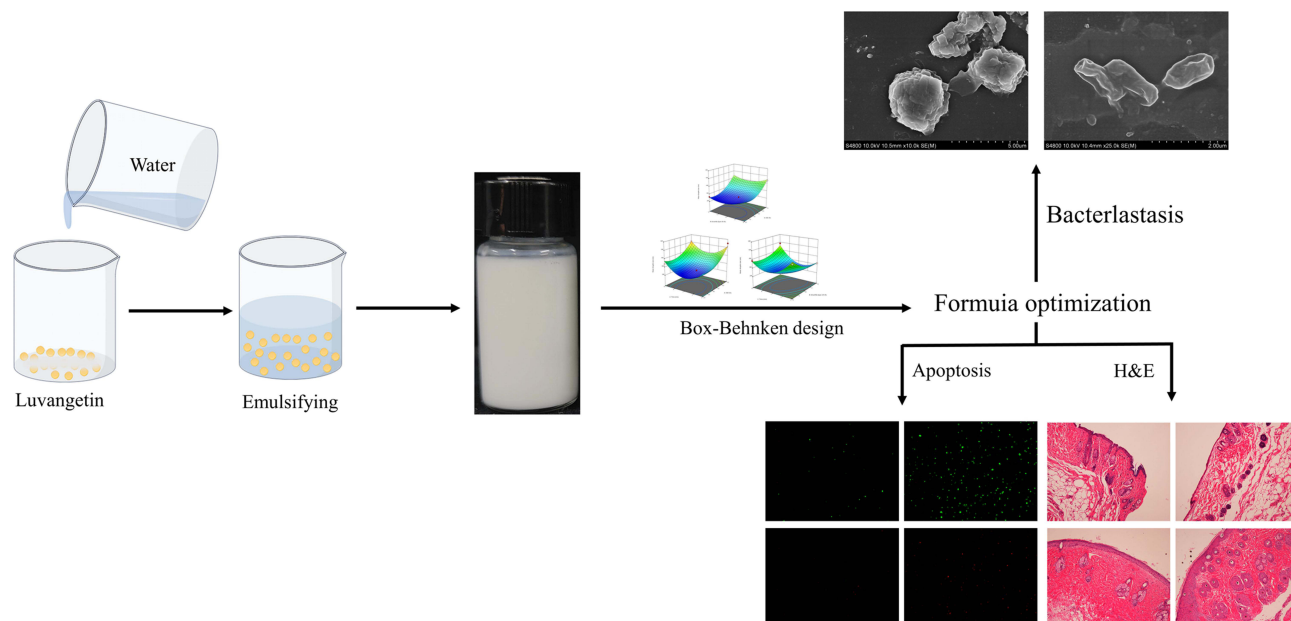
infections has emerged as an effective strategy. Currently, antimicrobial agents are primarily classified into synthetic antibiotics (such as β-lactams, including penicillin; cephalosporins; carbapenems; aminoglycosides; and sulfonamides) and certain inorganic materials (like micro or nanoscale forms of zinc (Zn), silver (Ag), copper (Cu), and gold (Au)).[8] Nonetheless, the use of various antibiotics at this stage can lead to adverse effects, including liver and kidney impairment, gastrointestinal reactions, dysbiosis, neurological reactions, and secondary infections,[9,10] while most inorganic materials are costly. Therefore, developing and applying novel antimicrobial agents has become both a trend and a necessity. For treating infected skin wounds, various wound dressings have been developed, including microneedle patches,[11] hydrogels,[12–14] and nanocomposite formulations.[15–17]

Coumarins and their derivatives exhibit diverse biological activities, including antitumor,[18] anti-HIV,[19] antibacterial and antifungal,[20,21] anti-inflammatory,[22,23] anticoagulant,[24] triglyceride-lowering,[25] and CNS stimulant effects.[26] Luvangetin, a linear pyranocoumarin and coumarin analog, possesses antioxidant, antibacterial, and antiviral properties.[27,28] It is commonly used in agricultural antimicrobial preparations, including a variety of plant extracts such as paramignya trimera,[29] pepper bark,[30] and eranthis longistipitata.[31] Currently, luvangetin is solely utilized in agricultural antimicrobial products,[30] highlighting a research gap in clinical antimicrobial applications. Therefore, we believe luvangetin exhibits antimicrobial effects against Gram-negative bacteria, presenting promising applications. However, given current technology, extracting natural plant monomers, such as high-purity luvangetin, is costly. Building on this, our organization's Chinese invention patent application (CN 115785113 A) reveals a method for synthesizing luvangetin, laying a solid groundwork for our research.

Nanoemulsions are colloidal delivery systems that have garnered significant attention owing to their high loading capacity and ability to effectively protect bioactive compounds. Nanoemulsion is a highly dispersed system formed by the combination of two immiscible substances, typically aqueous and oily phases, with a size range primarily between 20–500 nm. The appearance of nanoemulsion can be transparent or milky white, depending on the droplet size; smaller droplet sizes (usually less than 200 nm) tend to exhibit higher transparency.[32,33] Nanoemulsions offer several distinct advantages compared to other nanocarriers, including: (i) easy preparation and preservation; (ii) enhanced stability; and (iii) improved skin bioavailability.[33,34]

Currently, there is no research on the application of biological agents associated with luvangetin. For the first time, we have developed luvangetin nanoemulsions (LNs) by integrating the multifaceted, biologically active

coumarin analog luvangetin with nanoemulsion technology, a pioneering effort aimed at significantly enhancing the compounds' delivery efficiency and efficacy. In this study, luvangetin nanoemulsions (LNs) were prepared and their features were characterized, including physical appearance, average droplet size, polydispersity index (PDI), zeta potential, storage stability, and centrifugal stability to identify the best emulsifier. LNs formulation was optimized through Box-Behnken design (BBD), considering factors such as sunflower seed oil content, emulsifier concentration, and shear duration. Mean droplet size was used as the outcome measure. Furthermore, the efficacy of LNs against common nosocomial pathogens, specifically *MRSA* and *E. coli*, was evaluated. LNs biosafety was evaluated through cytotoxicity and apoptosis assays involving human epidermal and endothelial cells. Finally, the therapeutic effect of LNs on wound healing in mice infected with MRSA was studied in B6 mice. This study represents the first evaluation of LNs' safety using human epidermal and endothelial cells, as well as the inaugural in vivo application to assess their efficacy in treating infected wounds. It offers a novel direction for luvangetin's development and application.

Materials and Methods
Materials
Luvangetin (99% purity, obtained from the School of Pharmacy, Yangzhou University), Span series emulsifiers (Span-20, Span-40, Span-60, Span-80) obtained from Sinopharm Chemical Reagent Co., Ltd., Shanghai, China), sunflower seed oil (SSO) (food grade, Jager Foods Co., Ltd (TC), Suzhou, Jiangsu, China), *Methicillin-resistant Staphylococcus aureus, Staphylococcus aureus* and *Escherichia coli* strains (obtained from the Laboratory of the First Affiliated Hospital of Yangzhou University, China), ROS detection kit (AmyJet Science Inc., Wuhan, China), MDA detection kit (LAN Technology Co., Ltd., Beijing, China), CCK-8 cell viability assay kit (Baili (Beijing) Biotechnology Co., Ltd., Beijing, China), Annexin V-FITC/PI apoptosis detection kit (Baili (Beijing) Biotechnology Co., Ltd., Beijing, China), HaCat (obtained from XinRun Biotechnology Co., Ltd., Wuxi, China) and HUVEC (Chinese Academy of Sciences, Shanghai, China), 4–8 generations, B6 mice (obtained from the Institute of Comparative Medicine Experimental Animal Center, Yangzhou University, China).

Preparation of Nanoemulsions
The luvangetin was completely dissolved in DMSO to obtain a luvangetin solution with a mass fraction of 25%. The mixture of 2.5% sunflower seed oil (SSO) and 10% emulsifier was poured into a beaker, followed by the addition of a 3.25% Lujin ester solution. Water was added while mixing to reach a total mass of 10g. The final LNs were prepared by shearing the mixture using a rotor-stator homogenizer at 18,000 rpm for 7 minutes.[34] In O/W nanoemulsion, the use of an emulsifier can enhance the stability of the system.[33] Four distinct Span emulsifiers (Span-20, Span-40, Span-60, Span-80) were used to prepare the LNs, aiming to assess their impact on nanoemulsion stability. Resulting emulsions were designated as LN1, LN2, LN3, and LN4, in sequence.

Characterization of LNs
Average Droplet Size, PDI, and Zeta Potential
The mean droplet size, PDI, and Zeta potential of the newly formulated LNs were measured with a NanoSizer (ZS90 Nano, Malvern, UK). Three replicates were conducted to establish the mean value.[35,36]

Storage and Centrifugation Stability
The newly prepared LNs were aliquoted into 10 mL glass bottles and incubated at $54 \pm 2°C$ for seven days. The size of the newly prepared LNs and the samples after 7 days of thermal preservation were evaluated. In order to ensure centrifugation stability, 10 mL of LNs was transferred into a 15 mL centrifuge tube and centrifuged at a relative centrifugal force (RCF) of 2805g for a duration of 15 minutes. Distinct changes in appearance were observed before and after centrifugation.[37,38]

Optimization of LNs by BBD

The optimal formulation of LNs preparation was determined through pretesting and optimization using BBD. Independent factors including sunflower seed oil content (2.5%, 5.0%, 7.5%), emulsifier concentration (8%, 10%, 12%), and shear time (5, 7, 9 min) were evaluated, with the mean droplet size serving as the response variable.[39]

Antibacterial Activity of LNs

The diameter of the inhibition zone was assessed using the filter paper method, or agar disc method.[40] A bacterial suspension (*Methicillin-resistant Staphylococcus aureus (MRSA), S. aureus* and *E. coli*) was prepared, yielding a bacterial slurry, which was then diluted in phosphate-buffered saline (PBS) to an $OD_{600}= 0.5$. Subsequently, 100 μL of this bacterial solution was spread evenly over the surface of a solid Luria broth (LB) medium using a spreader. A sterile 6 mm filter paper disc was then placed on the medium surface with forceps and imbibed with 20 μL of the LNs solution. After inversion, the medium was incubated at 37°C for 24 hours. Post incubation, the diameter of the inhibition zone was recorded. For the control, SSO and dimethyl sulfoxide (DMSO) were used. In the case of the blank control, 100 μL of bacterial solution was spread on solid Luria broth (LB) medium.

Antibacterial Mechanisms of LNs

Morphological Analysis of the Bacteria

Cell culture coverslips were placed at the bottom of a six-well plate, and a bacterial suspension comprising *S. aureus* and *E. coli* (OD600= 0.5) was introduced. The cultures were incubated at 37°C for 6 hours. The cell climbing slices were transferred to a new 6-well plate and submerged in 2.0 mL of LNs to ensure complete coverage. They were then incubated at 37°C for 2 hours. Cell culture coverslips were then transferred to a new well, immersed in a 2.5% glutaraldehyde solution, and refrigerated at 4°C overnight. The adhered bacteria underwent graded dehydration through a graded series of ethanol solutions with concentrations of 30%, 50%, 70%, 80%, 90%, 95%, and 100%, each for 12 minutes. Following complete dehydration, the specimens were prepared and coated with gold to facilitate capturing of scanning electron microscopy (SEM) images.[34]

Analysis of Bacterial ROS

The bacterial suspensions of activated *S. aureus* and *E. coli* were thoroughly mixed with DCFH-DA and incubated in a 37°C incubator for 30 minutes. Subsequently, the suspensions were washed with PBS buffer and centrifuged three times. For the treatment group, 1 mL of LNs with a concentration of 3.84 mg/mL was added to the bacterial suspension. In contrast, the control group consisted of bacterial solutions without LN treatment. The samples were then distributed into 96-well plates, and reactive oxygen species (ROS) levels were determined using a spectrophotometer (Thermo Scientific Multiskan GO, USA). Fluorescence intensity changes were monitored at an excitation wavelength of 488 nm and an emission wavelength of 525 nm.[41]

Analysis of MDA

LNs (0.96, 1.92, 3.84 mg/mL) were incubated with the bacterial suspension for 30 minutes. The mixed solution, standard material, and water (200 μL in total) were combined in a 15 mL centrifuge tube. The prepared detection reagent was added to the tube, which was then thoroughly mixed by shaking. The centrifuge tube was incubated in a water bath at 95°C for 40 minutes, then removed and cooled in an ice bath before being centrifuged at 1785g for 10 minutes. Subsequently, the supernatant was discarded, and the absorbance of each tube was measured at 532 nm using a fluorescence spectrophotometer.[34]

Detection of Intracellular Lysate Leakage

The bacterial suspension containing activated *S. aureus* and *E. coli* was isolated in PBS and diluted to $OD_{600} = 0.5$. Afterwards, *S. aureus* and *E. coli* were treated with LNs at a concentration of 3.84 mg/mL and incubated at 37 °C. The bacterial suspension was collected, and after centrifugation, the supernatant was retained. The absorbance was measured at 0, 0.5, 1, 1.5, 2, 2.5, and 3 hours by using a fluorescence spectrophotometer to measure absorbance at 260 nm and 280 nm. The bacterial solutions without LNs served as the control group.[34,42]

Safety Evaluation of LNs
Cell Activity Evaluation
Cell Counting Kit-8 (CCK-8) was used to assess cell proliferation and cytotoxicity. HUVEC and HaCat were digested with trypsin and counted. Approximately 1000 cells were seeded into a 96-well plate with 100 μL of culture medium and incubated for 24 hours. Then, the medium containing serum was replaced with 90 μL of serum-free medium, and 10 μL of different concentrations of 60, 120, 240 and 480 μg/mL LNs solution was added for another 24-hour incubation. The serum-free medium was replaced with 90 μL per well, and 10 μL of CCK-8 solution was added. The plate was incubated at 37°C in a CO2 incubator for 4 hours, and the absorbance was measured at 450 nm using an Enzyme standard instrument (Thermo Scientific Multiskan GO, USA) reader.[42]

Analysis of Cell ROS
Cells were seeded in a 6-well plate and incubated until they completely covered the wells. Then, 100 μL of 0.2% H_2O_2 was added to induce cell damage. Meanwhile, the experimental group was treated with 100 μL of 240 μg/mL LNs solution. After co-culturing for 24 hours, DCFH-DA was diluted in serum-free medium at a ratio of 1:1000 to achieve a final concentration of 10 micromoles per liter. The culture medium was removed, and 1 mL of diluted DCFH-DA was added. The cells were incubated at 37°C for 20 minutes. After washing three times with serum-free cell culture medium, the fluorescence intensity was measured using an Enzyme standard instrument (Thermo Scientific Multiskan GO, USA) reader.

Cell Apoptosis
HaCat and HUVEC cells were cultured at 37°C in a CO2 incubator. The treatment group received LNs at 240 μg/mL, whereas the control group was exposed to 0.2% H2O2. Cells were treated with trypsin for 5 minutes before the enzyme was removed with a pipette. The cells were then washed with PBS, placed into a 2 mL centrifuge tube, and spun at 800 rpm for 4 minutes to pellet the cells. After discarding the supernatant, cells were resuspended in buffer. Next, both treated and control samples were stained with Annexin V-FITC and PI and then incubated at 25°C in the dark for 10 minutes. The samples were passed through a copper mesh filter, transferred to test tubes, and analyzed. Apoptotic cell death was assessed using a fluorescence microscope.

Evaluation of Wound Healing
All animal procedures and treatments adhered to relevant guidelines and were authorized by Yangzhou University's Animal Ethics Review Committee (License No. SCXK (Su)-2022-0044, certified by Jiangsu Province's Science and Technology Association). B6 mice, 4–6 weeks old, were selected from the same cohort. Following anesthesia with 100 μL of 1.5% pentobarbital solution via intraperitoneal injection under sterile conditions, a 1 cm diameter circular full-thickness wound was created on the back of each mouse with a sterile scalpel. Mice were then randomly assigned to two groups (n=3 each) and housed individually. Each mouse received 300 μL of 1x10⬚ CFU/mL MRSA suspension at the wound site on days 0 and 1 to induce infection. Subsequently, groups received PBS or 1.92 mg/mL LNs as treatment. Wound images were captured on days 1, 3, 5, and 7. Prior to imaging, the mice were restrained, and their wounds were purged using physiological saline. Tissue samples collected on day 8 for hematoxylin and eosin (H&E) staining and histological evaluation.[12]

Statistical Analysis
Each experiment was performed in triplicate and was averaged. Data were recorded as mean ± standard deviation (SD) for analysis of variance (ANOVA) using GraphPad 8.0.2 software.

Results and discussion
Selection of the Best Emulsifier for Formulation of LNs
The appearance of the newly prepared LNs is illustrated in Figure 1A. After the new preparation, LN 2 appears to be thick and hangs on the wall. LN 1, LN 3, and LN 4 are evenly distributed without any hanging or stratification. They
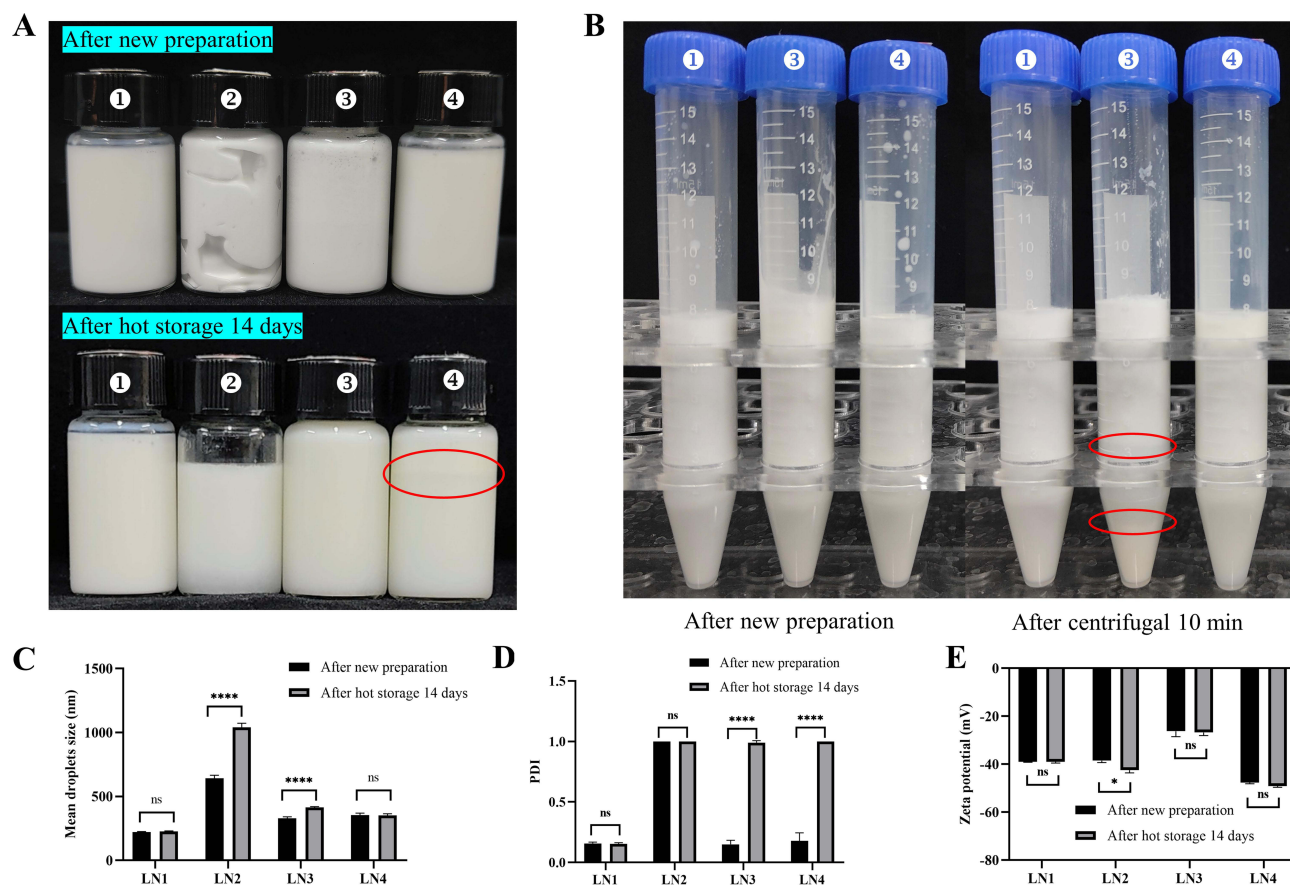
Figure 1 Characterization results of luvangetin nanoemulsions. (**A**) Storage stability (Red outlined circles: LN4 appears to be stratified, the upper layer of LN 4 became visible); (**B**) Centrifugal stability (Red outlined circles: After centrifugation, LN3 appeared stratified, significant stratification was observed in the bottom and middle parts); (**C**) Average droplet size; (**D**) PDI; (**E**) Zeta potential (ns, not statistically significant, *P < 0.05, ****P < 0.0001).

exhibit a rich milky white color and no blue light. After heating to $54 \pm 2°C$, the upper layer of LN 4 became visible. By observing the appearance of LN 3 before and after centrifugation (Figure 1B), significant stratification was observed in the bottom and middle parts. LN 1 and LN 4 remained unchanged, exhibiting a uniform color and no layers. Qualified nanoemulsion should remain stable and unlayered after centrifugation and heat storage. However, LN 2, LN 3, and LN 4 samples do not meet this criterion.

The average droplet size of LNs after new preparation and heat storage is presented in Figure 1C. The LN 2 sample has a large droplet size (> 500 nm), while LN 1, LN 3, and LN4 have an average droplet size < 500 nm. Among them, LN 1 has the smallest droplet size (< 300 nm). After 14 days of thermal storage, the size of all LNs increased. LN 2 showed the most significant change (P < 0.05), while LN 1 showed the least significant change (P > 0.05), remaining below 300 nm. The results indicate that the emulsifiers Span-20 (LN 1) and Span-80 (LN 4) exhibit superior emulsifying properties.

The PDI of LN 1, LN 3, and LN 4 in the newly prepared LNs was < 0.3 (Figure 1D), indicating excellent droplet dispersion. The PDI of LN 2, which reached 1.0, indicates poor stability. After thermal storage, the PDI of LNs increased. Among them, LN 3 and LN 4 showed the most significant increase (P< 0.0001), reaching 1.0, indicating poor stability. The PDI of LN 1 remained relatively unchanged before and after thermal storage, and the differences in PDI at different storage times were not statistically significant (P > 0.05).

An increase in droplet size is typically accompanied by an increase in the absolute zeta potential.[43] According to the Derjaguin-Landau-Verwey-Overbeek (DLVO) theory, a higher absolute value of the zeta potential on the droplet surface leads to increased electrostatic repulsion between droplets, resulting in more favorable droplet dispersion. This finding is consistent with previous studies.[35] All the formulated nanoemulsions exhibited a negative Zeta potential (< −50 mV)

(Figure 1E). After heat storage, the Zeta potential of LN 1, LN 3, and LN 4 did not show any statistically significant differences compared to the new preparation (P > 0.05).

This study aimed to prepare stable lipid nanoparticles (LNs) by optimizing the emulsifier formulation and selecting the optimal composition of Span-20. This approach avoided the complex process of emulsifier screening and effectively reduced the experimental time, while maintaining the quality of LNs.

Formula Optimization of LN by BBD

In prior research, the optimization of multiple factors influencing nanoemulsion formulation has frequently been approached through traditional univariate studies. This method simplifies the experimental design process but is typically limited to analyzing one factor at a time, failing to capture the interactions among all relevant factors.[44,45] BBD, an interplay of statistics and mathematics, enables the analysis and optimization of multiple independent variables on response values. It assesses the interactions between parameters and can significantly minimize the number of required experiments and the time devoted to extensive analysis.[46,47]

Applying BBD principles, we used SSO content (A), emulsifier content (B), and shear time (C) as independent variables, with the average LNs droplet size as the response variable. We designed 17 experiments to identify the optimal conditions for each factor (Table 1). ANOVA results for the quadratic regression response surface are detailed in Table 2. The subsequent multiple regression fitting—conducted with Design-Expert software—yielded an R-squared model equation of 0.9698 for the factors:

$$R=+234.44+83.44*A-14.43*B+10.6875*C+9.07*AB-12.45*AC+55.67*BC+76.46*A2+51.43*B2+121.51*C2$$

The corrected model demonstrates a strong fit and minimal experimental error, suitable for further analysis and predictive purposes. The ANOVA results for this equation can be found in Table 2. Upon comprehensive evaluation, factors A^2, B^2, and C^2 achieved highly significant levels (P < 0.01). Interaction terms for factors AC and BC showed significant differences (P < 0.05). No significant differences were observed in the interaction terms among factors A, B, and C. Furthermore, the model is considered significant, as indicated by an F-value of 24.94, confirming a good fit for the regression equation. The influence on the R value ranked as follows: A > B > C.

The response surface diagram for the secondary regression equation (Figure 2A–D) illustrates that with a fixed sunflower seed oil content, the R value decreases as the emulsifier amount increases, notably when it exceeds 10%. Similarly, at a fixed emulsifier content, the R value decreases with the increase in sunflower seed oil amount, showing insignificant changes when the sunflower seed oil content exceeds 2.5%. As shown in Figure 2B–E, with a fixed

Table 1 Experimental Design and Results of BBD Optimization for Luvangetin Nanoemulsions

Experiments	A (SSO %)	B (Emulsifier, Span-20%)	C (Time, min)	R (Mean droplet, size nm)
1	2.5	8	7	328.5
2	7.5	8	7	443.2
3	2.5	12	7	263.3
4	7.5	12	7	414.3
5	2.5	10	5	326.7
6	7.5	10	5	552.5
7	2.5	10	9	337.2
8	7.5	10	9	513.2
9	5	8	5	439.8
10	5	12	5	317.8
11	5	8	9	385.6
12	5	12	9	486.3
13	5	10	7	234.9
14	5	10	7	236.7
15	5	10	7	232.3
16	5	10	7	238.8
17	5	10	7	229.5

Table 2 The Analysis of Variance for Quadratic Regression Equation of Response Surface

Source	df	Mean Square	F-value	p-value
Model	9	19,918.99	24.94	0.0002
A	1	55,694.53	69.73	< 0.0001
B	1	1664.64	2.08	0.1921
C	1	913.78	1.14	0.3203
AB	1	329.42	0.4124	0.5412
AC	1	620.01	0.7763	0.4075
BC	1	12,398.82	15.52	0.0056
A²	1	24,612.07	30.82	0.0009
B²	1	11,137.03	13.94	0.0073
C²	1	62,161.96	77.83	< 0.0001
Residual	7	798.7		
Lack of Fit	3	1845.86	138.49	0.0002
Pure Error	4	13.33		
Cor Total	16			

sunflower seed oil content, the R value gradually decreases with increasing shear times, and it starts to increase slowly when the shear time exceeds 7 min. Conversely, at a fixed shear time, the R value decreases with higher sunflower seed oil content. From Figure 2C–F, at a fixed emulsifier content, the R value gradually decreases with increasing shear times, and it starts to decrease slowly when the shear time exceeds 7 min. Moreover, at a certain shear time, the R value decreases gradually when the emulsifier exceeds 10%.

The factor A surface is markedly steep, indicating a significant impact on the response value; factors B and C follow in terms of influence. Contour plots reveal near-elliptical shapes, which signify strong interactions among the three
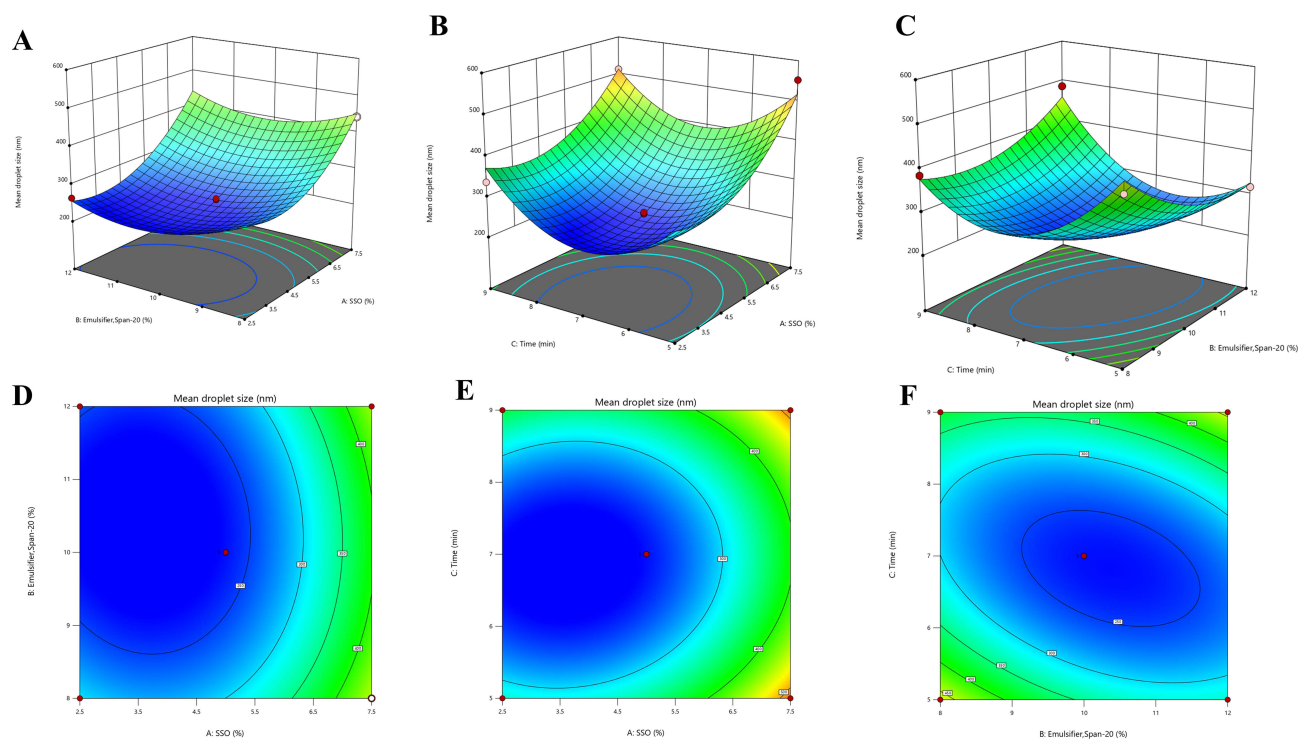

Figure 2 Response surface diagrams for preparation of luvangetin nanoemulsions. (**A**–**D**) sunflower seed oil and emulsifier content; (**B**–**E**) sunflower seed oil content and shear time; (**C**–**F**) emulsifier content and shear time (Red dots: fixed central values of factors, yellow dots: extreme combinations of factor levels).

Table 3 Verification Experiment for Evaluating Predicted/Actual R Values in Luvangetin Nanoemulsions

Experiments	Predicted value	Actual value	Average value	RSD (%)
1	225.6	228.9	227.7	1.17
2		224.7		
3		229.3		

factors. According to Design-Expert software, the optimal LNs formulation contains 2.5% sunflower seed oil, 9.994% Span-20 emulsifier, and a shear duration of 7.034 minutes. In light of practical applications, the final formula was adjusted to 2.5% sunflower seed oil, a rounded 10% emulsifier, and a shear duration of 7 minutes.

The predicted R value for the optimal LN formulation was 226 nm. Subsequently, LNs were prepared based on this optimized formulation, and three validation tests were conducted. The results (Table 3) revealed that the average droplet sizes of the prepared LNs were 228.9 nm, 224.7 nm, and 229.3 nm, with a relative error of 1.17% compared to the predicted value. These findings indicate the stability, reliability, and reproducibility of the optimized LN formulation.

Results of the Antibacterial Activity of the LNs

According to the drug susceptibility measurement criteria, the bacteria can be classified as sensitive to the drug.[48] The agar disk method demonstrated the high sensitivity of LNs to two standard strains, namely *S. aureus, MRSA* and *E. coli*. Among them, LNs exhibited significantly stronger inhibition against *S. aureus* and *MRSA* compared to *E. coli*. As depicted in Figure 3A and B, increasing the concentration of luvangetin (LNa, LNb, LNc, and LNd concentrations were 0.96, 1.92, 3.84, and 7.69 mg/mL, respectively) resulted in a corresponding enhancement of the antibacterial effect.

Antibacterial Mechanisms of LNs

Antimicrobial mechanisms of LNs for *S. aureus* and *E. coli* are shown in Figures 4 and 5. Scanning electron microscopy (SEM) images in Figures 4A and 5A demonstrate that untreated *S. aureus* exhibits intact, smooth, and round characteristics, while *E. coli* appears as straight rods. On the other hand, as depicted in Figures 4B and 5B, *S. aureus* treated with LNs exhibits a convex, distorted, or cracked morphology, while *E. coli* shows an irregular and concave shape. Figures 4C and 5C demonstrate significantly higher levels of reactive oxygen species (ROS) in LNs-treated *S. aureus* and *E. coli* compared to the control group at the same treatment time ($P < 0.0001$). Figures 4D and 5D show that the treatment group's MDA levels were significantly elevated compared to the control group, with *S. aureus* levels peaking at 89 nmol/mL and *E. coli* levels at
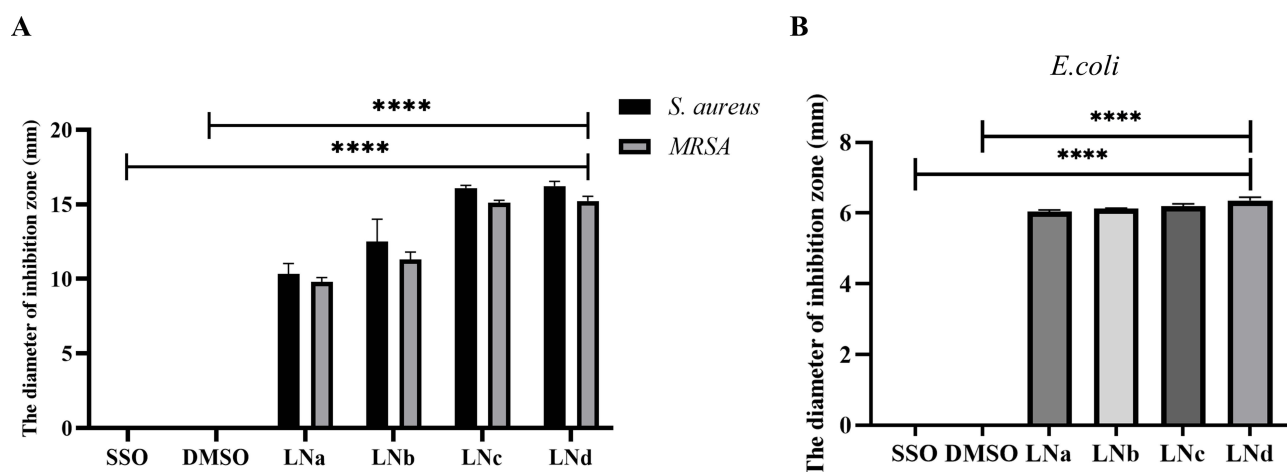
Figure 3 Inhibition zone diameter of luvangetin nanoemulsions. (**A**) *S. aureus* and *MRSA*; (**B**) *E. coli* (**** P < 0.0001).
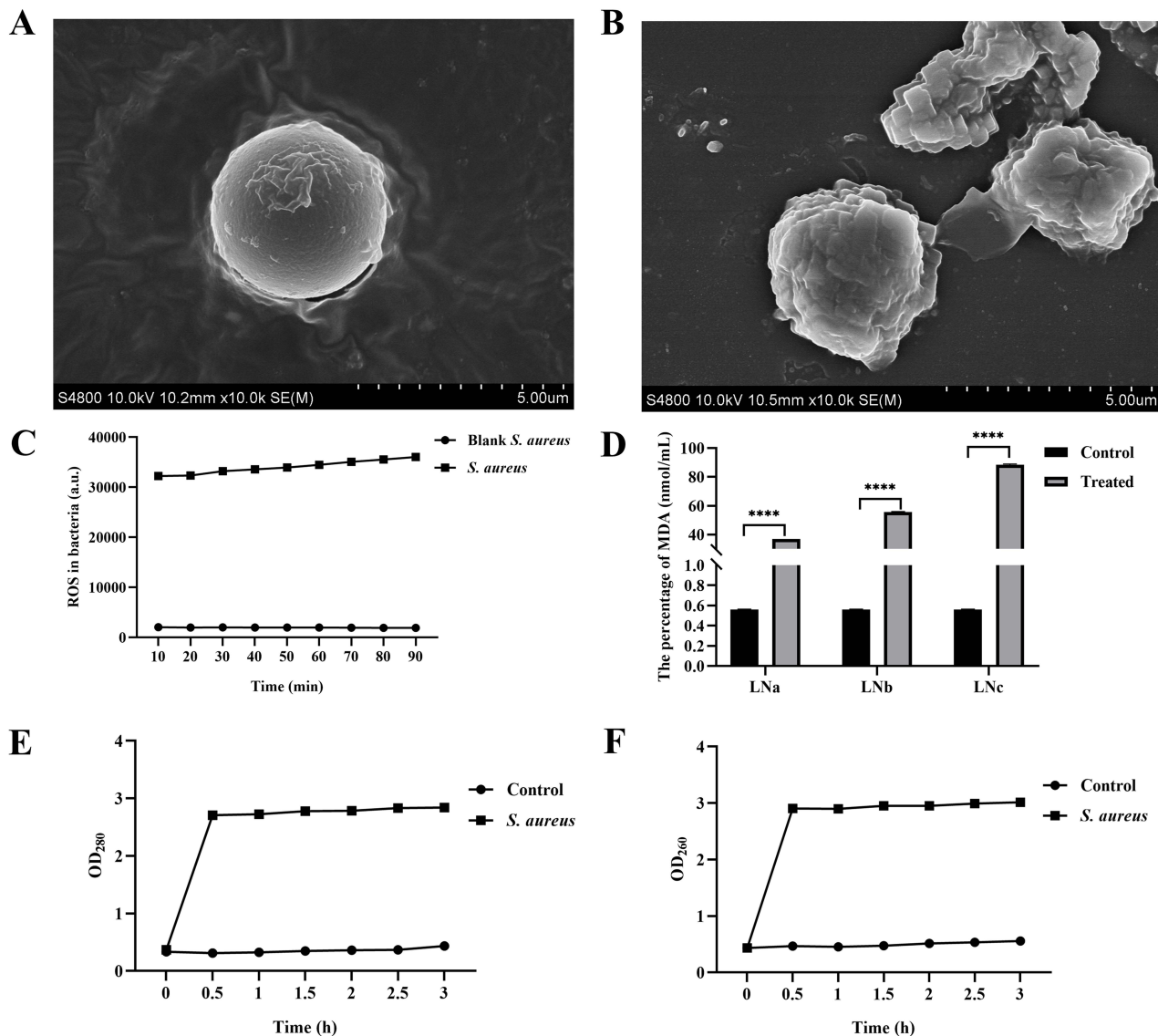
Figure 4 Antimicrobial mechanism of luvangetin nanoemulsion against *S. aureus*. (**A**) (**B**) SEM; (**C**) ROS. The level of ROS in the bacteria after LNs treatment was significantly different from that in the blank group (P < 0.0001); (**D**) MDA. The differences between the groups and the standard control group at different concentrations were significant (**** P < 0.0001); (**E**) (**F**) intracellular lysate leakage. The LNs OD280 and OD260 of *S. aureus* after treatment were statistically different from the blank group (P < 0.05).

94 nmol/mL. There were significant differences in MDA levels between different LNs concentrations and the control group for the same organism (P <0.0001).

Figure 4E and F and Figure 5E and F display the solute leakage of LNs-treated bacteria over time. Post-LNs treatment, significant differences in OD_{260} and OD_{280} from the blank group were observed (P < 0.05). In the blank group, solute leakage was consistently near zero, indicating minimal cell damage in untreated bacteria. Following treatment with 3.84 mg/mL of LNs, changes in solute leakage were noted: a rapid increase in nucleic acids leakage within the first 0.5 hours, followed by a plateau. Within 0.5 hours of LN treatment, the OD_{260} for the S. aureus group rose from 0.435 to approximately 3.020, while the E. coli group's OD_{260} rose from 0.40 to about 3.10. From 1.0 to 3.0 hours post-treatment, all groups showed a slower increase in OD_{260}. Similarly, within the initial 0.5 hours, the OD_{280} for *S. aureus* spiked from 0.370 to roughly 2.840, and for *E. coli*, from 0.282 to approximately 2.920.
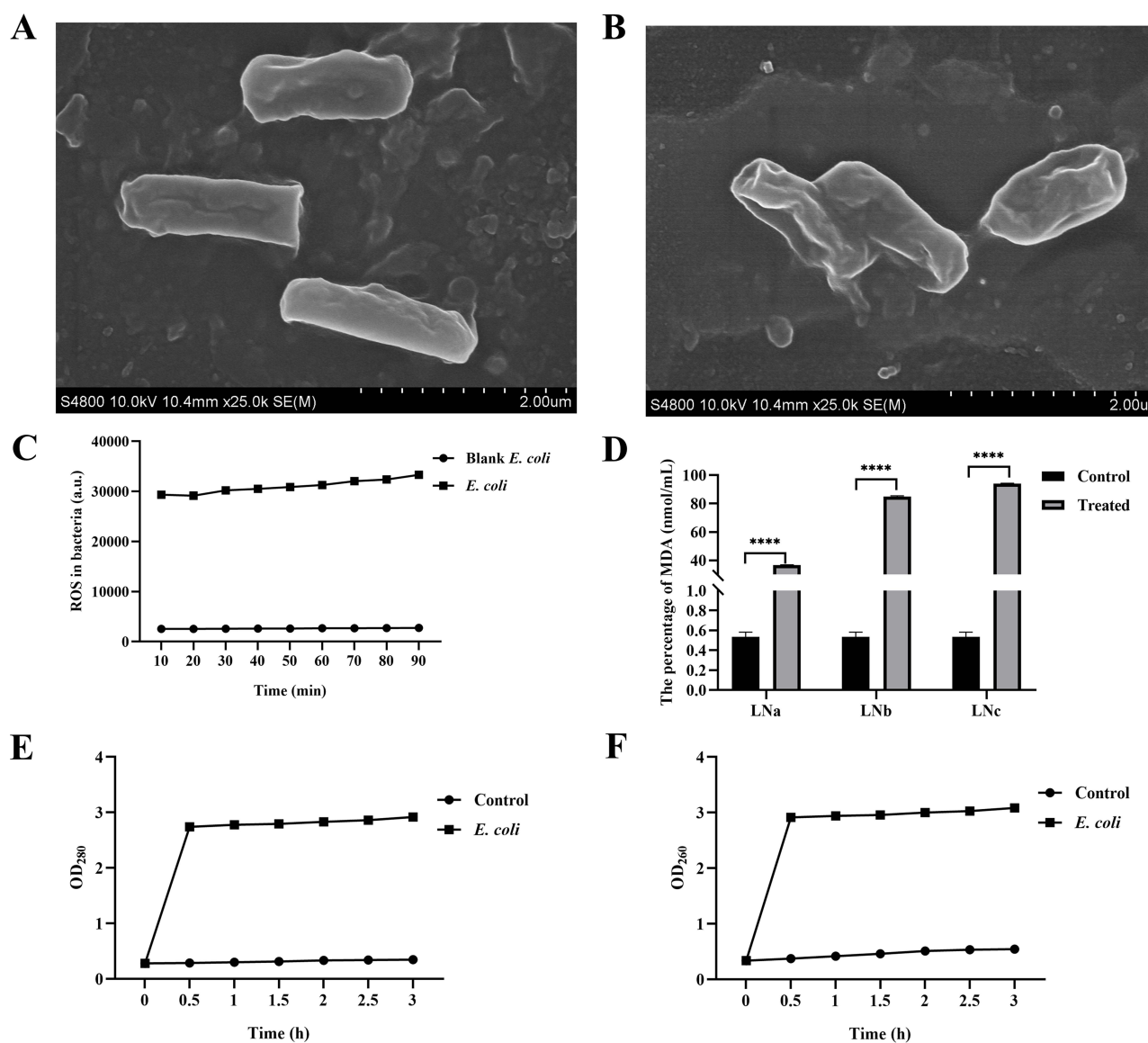
Figure 5 Antimicrobial mechanism of luvangetin nanoemulsion against *E. coli*. (**A**) (**B**) SEM; (**C**) ROS. The level of ROS in the bacteria after LNs treatment was significantly different from that in the blank group ($P < 0.0001$); (**D**) MDA. The differences between the groups and the standard control group at different concentrations were significant (**** $P < 0.0001$); (**E**) (**F**) intracellular lysate leakage. The LNs OD280 and OD260 of *E. coli* after treatment were statistically different from the blank group ($P < 0.05$).

Cellular Biosafety Results for the LNs

After 24 hours of treatment with 60, 120, 240, and 480 μg/mL LNs on HaCat and HUVEC, the cell survival rates were all >100% (Figure 6A) (HaCat, $P < 0.01$, HUVEC, $P < 0.0001$, respectively). Two groups of HaCat and HUVEC were injured by 0.2% H_2O_2, and a decrease in cellular ROS was observed after treatment with 240 μg/mL LNs (Figure 6B). Compared to HUVEC, LNs had a better therapeutic effect on HaCaT, indicating that LNs can reduce ROS produced by injured HaCat and HUVEC at a certain concentration. In the apoptosis experiment, when Annexin V-FITC and PI were used together, viable cells and early apoptotic cells were excluded by FITC and PI double staining, while late apoptotic cells and necrotic cells were stained green-blue and red, respectively (Figure 6C). The ratio of apoptosis to cell death in the HaCat treatment group compared to the positive control group was 21.39% and 40.13% ($P < 0.001$), respectively (Figure 6D). The ratio of apoptosis to cell death in the HUVEC treatment group compared to the positive control group was 29.16% and 18.54% ($P < 0.01$), respectively.
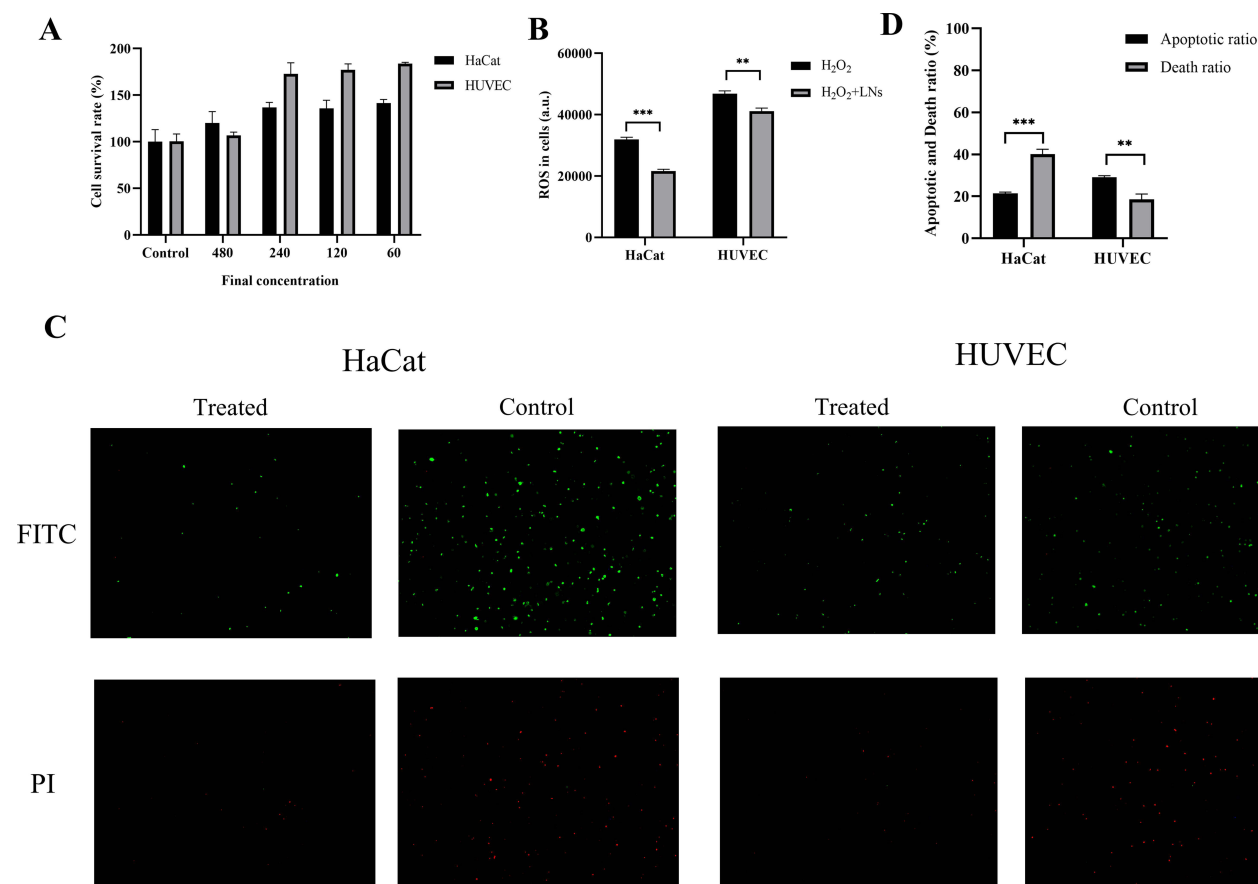
Figure 6 Effects of luvangetin nanoemulsions on HaCat and HUVEC. (**A**) Cell survival. Significant differences in cell viability between HaCat and HUVEC cell treated groups and control group at different concentrations of LNs (HaCat, P < 0.01, HUVEC, P < 0.0001); (**B**) Cellular ROS. ROS values before and after treatment of different damaged cells by LNs (HaCat, *** P < 0.001; HUVEC, ** P < 0.01); (**C**) Fluorescence microscope observation of pictures of different cells treated group and positive control group; (**D**) Apoptosis ratio and cell death ratio (HaCat, *** P < 0.001; HUVEC, ** P < 0.01).

Evaluation of LNs on Infectious Wound Healing in Mice

To evaluate the effects of LNs on actual infected wound healing in vivo, we utilized a B6 mouse model (Figure 7). Skin wounds with a diameter of approximately 1cm were created on the backs of the mice and infected with MRSA. The mice were then divided into a PBS control group and an LNs treatment group. During the treatment period, photographs of the skin wounds were taken four times (Figure 7B). In the PBS control group, the wound area decreased by 18.2%, 28.4%, and 38.8% on the 3rd, 5th, and 7th day, respectively. In contrast, in the LNs treatment group, the decrease in wound area exceeded 38.6%, 63.2%, and 72.9% on the corresponding days (Figure 7C). Compared to PBS, the LNs treatment group exhibited satisfactory wound healing ability (Figure 7B and C). On the 8th day, the wound tissues were analyzed histologically using H&E staining. As shown in Figure 7D, the wounds treated with LNs displayed a significant reduction in inflammatory cells, abundant neovascularization, noticeable sloughing of necrotic tissue, multilayered epithelial cell coverage, increased epidermal thickness, orderly collagen protein, enhanced differentiation of newly formed collagen fibers, and regeneration of skin appendages. However, in the PBS group, only tissue damage and relatively intact epidermis with few neovascularizations could be observed.

Discussion

The presented results highlight the significant impact of emulsifier type on the stability of LNs.[49] Choosing an optimal emulsifier is vital for creating stable nanoemulsions. To assess emulsifier performance, we measured mean droplet size, PDI, zeta potential, and both storage and centrifugal stabilities. LN 4, made with Span-80, demonstrated significant droplet size variance after thermal treatment and centrifugation. Meanwhile, LN 2, formulated with Span-40, presented
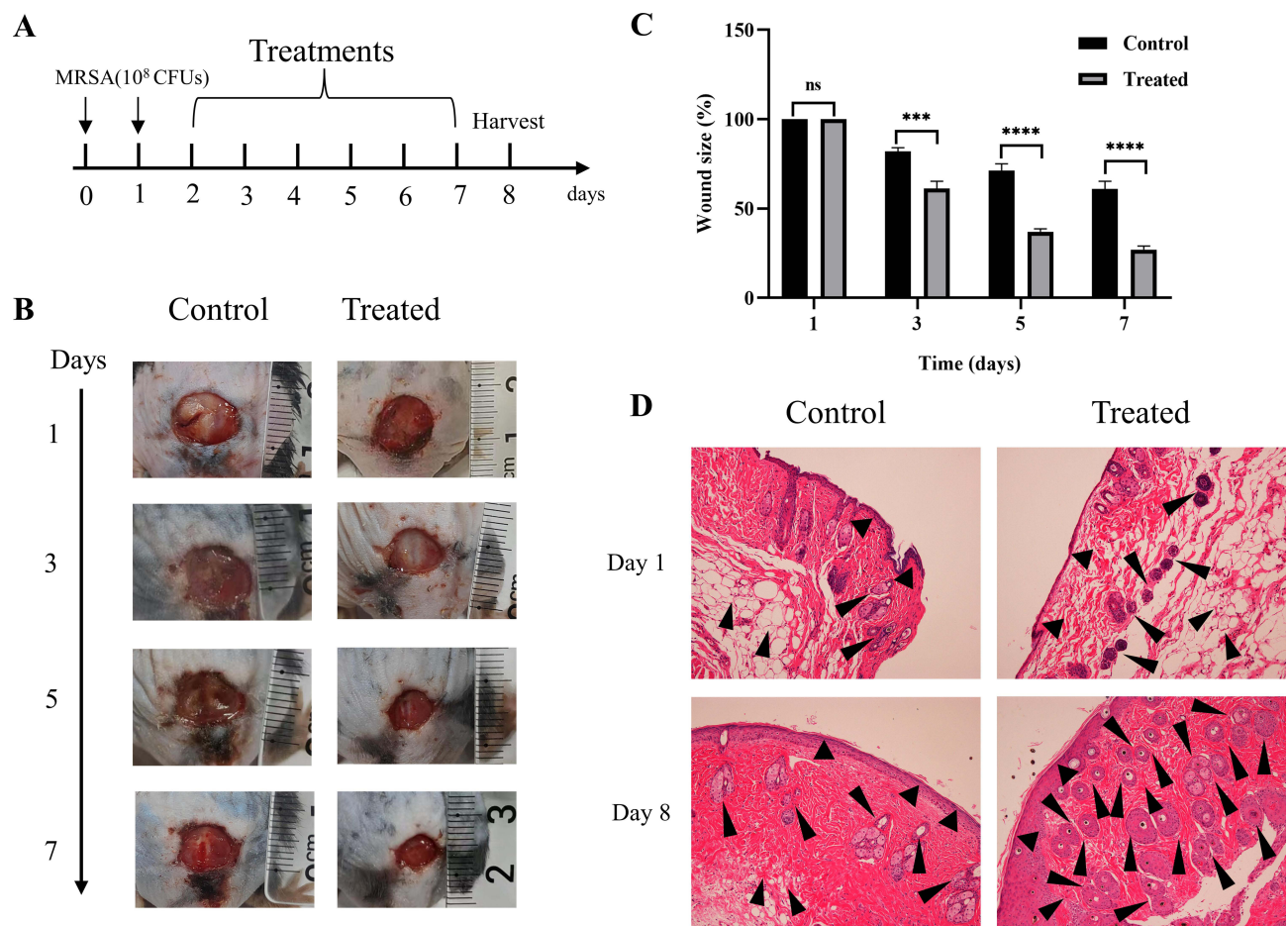
Figure 7 In vivo antimicrobial activity of luvangetin nanoemulsion. (**A**) Schematic of wound infection model and treatment protocol. (**B**) and (**C**) Changes in wound area and size (ns, not statistically significant, *** $p < 0.001$, **** $p < 0.0001$). (**D**) (**H** and **E**) staining results of wound tissues before and after infection after different treatment regimens (Black arrows at different scales:The areas of rich capillaries, granulation tissue, and collagen).

with a pronounced thickening and creaming effect. Conversely, LN 1 produced with Span-20 yielded droplets that were small, uniformly dispersed, and exhibited good stability.

This study focused on optimizing LNs using the Box-Behnken design (BBD). Key parameters like mean droplet size, PDI, and stability factors were characterized, identifying Span-20 as the ideal emulsifier. The optimal LNs formulation was achieved with a composition of 2.5% sunflower oil, 10% Span-20 emulsifier, and a shear time of 7 minutes, demonstrating the effectiveness of the BBD approach in LNs development. Oil-in-water nanoemulsions enhance the skin's absorption of active ingredients due to their internal lipophilicity.[50] Their small particle size results in a larger specific surface area, facilitating greater transdermal absorption.[51] Thus, nanoemulsions hold promise for topical drug delivery. Additionally, we achieved the production of a stable LNs, free from flocculation and delamination, through formulation screening and BBD optimization to ensure stability. Furthermore, the high yield of luvangetin was derived from the pepper species Zanthoxylum avicennae.[52] In recent years, research on the convergence of medicine and food has advanced.[53] The oil phase in the formulation consisted of sunflower seed oil, ensuring product biosafety. The affordability and efficacy of LNs make it a viable option for widespread use.

We assessed the antimicrobial activity of LNs using the agar diffusion method. Decreasing the droplet size of LNs through high-speed shear facilitates the rapid penetration of luvangetin into the bacterial cell membrane, enabling more efficient entry into the cell and enhancing its antibacterial effect. The results of SEM revealed that LNs caused significant damage to the bacterial cell wall, particularly on *S. aureus*. LNs have the ability to penetrate the cell wall and disrupt membrane structures, potentially resulting in cell lysis. DCFH-DA, a non-fluorescent compound, readily traverses the

cell membrane. Once inside the cell, it is hydrolyzed by intracellular esterases, producing DCFH. Since DCFH is unable to penetrate the cell membrane, loading the probe into the cell is straightforward. Intracellular ROS oxidizes the non-fluorescent DCFH, resulting in the production of fluorescent DCF.[54] Thus, measuring DCF fluorescence indicates cellular ROS levels. Elevated ROS levels arise from bacterial damage, and excessive ROS further accelerates damage and leads to bacterial death.[55] Malondialdehyde (MDA) levels act as indicators of lipid peroxidation rate and intensity, offering an indirect reflection of tissue peroxidative damage.[56] Higher concentrations of LNs corresponded to higher MDA content, indicating increasingly severe bacterial damage. LNs disrupt bacterial cell membrane structure, causing damage and oxidative stress. They also increase ROS levels, enhancing lipid peroxidation and resulting in increased MDA. Elevated MDA levels can interfere with bacterial metabolism and intensify damage. Bacterial intracellular leakage, a key parameter for assessing cell damage,[57] was measured by nucleic acid and protein leakage to evaluate LNs' impact. The data demonstrate that LNs compromise bacterial cytoplasmic membrane integrity, resulting in intracellular substance leakage. Luvangetin, a monoterpenoid phenolic compound—may cause this effect by decomposing and dissolving membrane lipids, thereby directly impairing cell membrane integrity.

HaCat cells, predominant in human skin, are crucial for wound healing, particularly in re-epithelialization.[58–60] Similarly, capillaries provide nutrient support for granulation tissue formation, while HUVECs are key to angiogenesis.[58,61] To evaluate the potential of LNs, we employed the CCK-8 assay to assess their impact on HaCat and HUVEC cell lines. Cell toxicity—manifested as cell death, lysis, or growth inhibition due to chemicals—serves as a crucial measure of cell viability. The cell survival rate is inversely proportional to the cytotoxicity of the tested formulation. Indicating that LNs have no toxicity on HaCat and HUVEC at lower concentrations and, conversely, have a certain proliferative effect. However, at higher concentrations, LNs exhibit a certain toxic effect on HaCat and HUVEC, indicating that LNs can be applied for disinfection and sterilization within an appropriate concentration range, while also having the potential to promote wound healing. Excessive ROS in bacteria accelerates damage and induces death; similarly, high ROS levels are detrimental to cells.[62] Research indicates that at specific concentrations, LNs mitigate HaCat damage and ROS production by HUVECs. This suggests LNs, within these concentrations, are effective for both disinfection and wound healing by minimizing cellular damage.LNs exhibit low cytotoxicity and high biocompatibility at low bacteriostatic concentrations, indicating that they are stable and safe for future use.

Wound healing encompasses biological processes including vascular regeneration, inflammatory response, and collagen formation.[12] Chronic wounds, marked by enduring inflammation and ongoing infection, pose significant challenges to healing,[63] and remain a concern for clinicians. Adequate vascularization, by delivering nutrients and oxygen, promotes wound healing.[14] Similarly, collagen deposition influences both the completeness of wound healing and scar formation.[12] MRSA infection is more likely to result in chronic wounds.[64] Our study revealed that mice treated with LNs exhibited a relatively high rate of wound healing. The healed tissues had more neovascularized capillaries and a more perfected epidermis, as observed by HE staining, highlighting LNs' potential as a treatment for clinical infectious wound healing.

Conclusion

We combined luvangetin, a multifunctional coumarin analog, with nanoemulsions. This combination offers a novel approach to topical bactericidal formulations, leveraging the antimicrobial properties of luvangetin for enhanced biocidal and disinfectant roles. This study employed nanoemulsions, a cutting-edge drug delivery technology, to transform luvangetin—a underutilized compound—into a practical bioactive formulation. The increased particle size in nanoemulsions enhances the contact surface area, surpassing that of existing drug formulations, thereby improving drug efficacy. In conclusion, nanoemulsions have been demonstrated to outperform other formulations in efficacy, safety, permeability, and bioavailability.[65] This not only broadens luvangetin's applications but also introduces innovative concepts and solutions for antimicrobial and therapeutic areas. The findings hold significant implications for the further application and development of luvangetin.

Data Sharing Statement

Data will be made available on request from corresponding author.

Ethical Statement

This study and the included experimental procedures were approved by the Institutional Animal Care and Use Committee of Yangzhou University (License No. SCXK (Su)-2022-0044, certified by Jiangsu Province's Science and Technology Association). All animal housing and experiments were conducted in strict accordance with the institutional guidelines for the care and use of laboratory animals.

Acknowledgments

Author Contributions

All authors made a significant contribution to the work reported, whether that is in the conception, study design, execution, acquisition of data, analysis and interpretation, or in all these areas; took part in drafting, revising or critically reviewing the article; gave final approval of the version to be published; have agreed on the journal to which the article has been submitted; and agree to be accountable for all aspects of the work.

Disclosure

The authors have no relevant financial or non-financial interests to disclose.

References

1. Baron JM, Glatz M, Proksch E. Optimal support of wound healing: new insights. dermatology. *Basel Switzerland*. 2020;236(6):593–600. doi:10.1159/000505291
2. Brem H, Tomic-Canic M. Cellular and molecular basis of wound healing in diabetes. *J Clin Invest*. 2007;117(5):1219–1222. doi:10.1172/jci32169
3. Harding KG, Morris HL, Patel GK. Science, medicine and the future: healing chronic wounds. *BMJ*. 2002;324(7330):160–163. doi:10.1136/bmj.324.7330.160
4. Bishop A. Role of oxygen in wound healing. *J Wound Care*. 2008;17(9):399–402. doi:10.12968/jowc.2008.17.9.30937
5. Edwards R, Harding KG. Bacteria and wound healing. *Curr Opin Infect Dis*. 2004;17(2):91–96. doi:10.1097/00001432-200404000-00004
6. Canchy L, Kerob D, Demessant A, Amici JM. Wound healing and microbiome, an unexpected relationship. *J Europe Acad Derma Vene*. 2023;37 (Suppl 3):7–15. doi:10.1111/jdv.18854
7. Olsson M, Järbrink K, Divakar U, et al. The humanistic and economic burden of chronic wounds: a systematic review. *Wound Rep Rege*. 2019;27 (1):114–125. doi:10.1111/wrr.12683
8. Guo Z, Chen Y, Wang Y, Jiang H, Wang X. Advances and challenges in metallic nanomaterial synthesis and antibacterial applications. *J Mat Chem B*. 2020;8(22):4764–4777. doi:10.1039/d0tb00099j
9. Björnsson ES. Drug-induced liver injury due to antibiotics. *Scand J Gastroenterol*. 2017;52(6–7):617–623. doi:10.1080/00365521.2017.1291719
10. Rouveix B. Antibiotic safety assessment. *Int J Antimicrob Agents*. 2003;21(3):215–221. doi:10.1016/s0924-8579(02)00354-0
11. Sun M, Zhong X, Dai M, et al. Antibacterial microneedle patch releases oxygen to enhance diabetic wound healing. *Mater Today Bio*. 2024;24:100945. doi:10.1016/j.mtbio.2024.100945
12. Yang P, Ju Y, Liu X, et al. Natural self-healing injectable hydrogels loaded with exosomes and berberine for infected wound healing. *Mater Today Bio*. 2023;23:100875. doi:10.1016/j.mtbio.2023.100875
13. Sun C, Liu W, Wang L, et al. Photopolymerized keratin-PGLa hydrogels for antibiotic resistance reversal and enhancement of infectious wound healing. *Mater Today Bio*. 2023;23:100807. doi:10.1016/j.mtbio.2023.100807
14. Jiang Y, Cao Y, Wu J, et al. Au nanozyme-based multifunctional hydrogel for inflammation visible monitoring and treatment. *Mater Today Bio*. 2024;25:100960. doi:10.1016/j.mtbio.2024.100960
15. Dědková K, Janíková B, Matějová K, et al. Preparation, characterization and antibacterial properties of ZnO/kaoline nanocomposites. *J Photochem Photobiol B Biol*. 2015;148:113–117. doi:10.1016/j.jphotobiol.2015.03.034
16. Zhang Z, Zhao Y, Hu Z, Si Z, Yang Z. 2-Pyridinecarboxaldehyde-modified chitosan-silver complexes: optimized preparation, characterization, and antibacterial activity. *Molecules*. 2023;28(19). doi:10.3390/molecules28196777
17. Wang C, Liu W, Cao H, Jia L, Liu P. Cellulose nanofibers aerogels functionalized with AgO: preparation, characterization and antibacterial activity. *Int J Biol Macromol*. 2022;194:58–65. doi:10.1016/j.ijbiomac.2021.11.164
18. Küpeli Akkol E, Genç Y, Karpuz B, Sobarzo-Sánchez E, Capasso R. Coumarins and coumarin-related compounds in pharmacotherapy of cancer. *Cancers*. 2020;13(7):12. doi:10.3390/cancers12071959
19. Kostova I, Momekov G, Tzanova T, Karaivanova M. Synthesis, characterization, and cytotoxic activity of new lanthanum(III) complexes of bis-coumarins. *Bioi Chem Appl*. 2006;2006:25651. doi:10.1155/bca/2006/25651

20. Musicki B, Periers AM, Laurin P, et al. Improved antibacterial activities of coumarin antibiotics bearing 5',5'-dialkylnoviose: biological activity of RU79115. *Bioorg Med Che Lett*. 2000;10(15):1695–1699. doi:10.1016/s0960-894x(00)00304-8

21. Al-Haiza MA, Mostafa MS, El-Kady MY. Synthesis and biological evaluation of some new coumarin derivatives. *Molecules*. 2003;8(2):275–286. doi:10.3390/80200275

22. Fylaktakidou CK, Hadjipavlou-Litina JD, Litinas EK, Nicolaides ND. Natural and synthetic coumarin derivatives with anti-inflammatory / antioxidant activities. *Curr Pharm Des*. 2004;10(30):3813–3833. doi:10.2174/1381612043382710

23. Tosun A, Akkol EK, Yeşilada E. Anti-Inflammatory and antinociceptive activity of coumarins from seseli gummiferum subsp. corymbosum (Apiaceae). *Zeitschrift für Naturforschung C*. 2009;64(1–2):56–62. doi:10.1515/znc-2009-1-210

24. Hoult JRS, Payá M. Pharmacological and biochemical actions of simple coumarins: natural products with therapeutic potential. *General Pharma*. 1996;27(4):713–722. doi:10.1016/0306-3623(95)02112-4

25. Madhavan GR, Balraju V, Mallesham B, Chakrabarti R, Lohray VB. Novel coumarin derivatives of heterocyclic compounds as lipid-Lowering agents. *Bioorg Med Che Lett*. 2003;13(15):2547–2551. doi:10.1016/S0960-894X(03)00490-6

26. Moffett RB. Central nervous system depressants. VII.1 pyridyl coumarins. *J Med Chem*. 1964;7(4):446–449. doi:10.1021/jm00334a010

27. Xiong Y, Huang G, Yao Z, et al. Screening effective antifungal substances from the bark and leaves of Zanthoxylum avicennae by the bioactivity-guided isolation method. *Molecules*. 2019;24(23):4207. doi:10.3390/molecules24234207

28. Niu XM, Li SH, Peng LY, Lin ZW, Rao GX, Sun HD. Constituents from Limonia crenulata. *J Asian Nat Prod Res*. 2001;3(4):299–311. doi:10.1080/10286020108040370

29. Tuan Anh HL, Kim D-C, Ko W, et al. Anti-inflammatory coumarins from Paramignya trimera. *Pharm Biol*. 2017;55(1):1195–1201. doi:10.1080/13880209.2017.1296001

30. Xiong Y, Huang G, Yao Z, et al. Screening effective antifungal substances from the bark and leaves of Zanthoxylum avicennae by the bioactivity-guided isolation method molecules. 2019;1:1.

31. Erst AS, Chernonosov AA, Petrova NV, et al. Investigation of chemical constituents of eranthis longistipitata (Ranunculaceae): coumarins and furochromones. *Int J Mol Sci*. 2022;23(1):406. doi:10.3390/ijms23010406

32. Klang V, Matsko NB, Valenta C, Hofer F. Electron microscopy of nanoemulsions: an essential tool for characterisation and stability assessment. *Micron*. 2012;43(2):85–103. doi:10.1016/j.micron.2011.07.014

33. Tadros T, Izquierdo P, Esquena J, Solans C. Formation and stability of nano-emulsions. *Adv Colloid Interface Sci*. 2004;108-109:303–318. doi:10.1016/j.cis.2003.10.023

34. Liu Q, Wang Z, Mukhamadiev A, et al. Formulation optimization and characterization of carvacrol-loaded nanoemulsions: in vitro antibacterial activity/mechanism and safety evaluation. *Ind Crops Prod*. 2022;181:114816. doi:10.1016/j.indcrop.2022.114816

35. Liu Q, Gao Y, Fu X, et al. Preparation of peppermint oil nanoemulsions: investigation of stability, antibacterial mechanism and apoptosis effects. *Colloids Surf B*. 2021;201:111626. doi:10.1016/j.colsurfb.2021.111626

36. Cadogan SP, Hahn CJ, Rausch MH, Fröba AP. Study on the applicability of dynamic light scattering (DLS) to microemulsions including supercritical carbon dioxide-swollen micelles. *J Colloid Interface Sci*. 2017;499:202–208. doi:10.1016/j.jcis.2017.03.111

37. Yuliani S, Muchtadi TR, Syakir M. Changes in characteristics of nanoemulsion of cinnamon oil and their relationships with instability mechanisms during storage. *J Food Process Preserv*. 2018;42(10):e13745. doi:10.1111/jfpp.13745

38. SA P, Kate V. Goodness of fit model dependent approach for release kinetics and in vitro release of piroxicam from PEGS based non aqueous emulsion. *Inventi Rap*. 2012;1:1

39. Shirasangi R, Kohli HP, Gupta S, Chakraborty M. Separation of methylparaben by emulsion liquid membrane: optimization, characterization, stability and multiple cycles studies. *Colloids Surf A*. 2020;597:124761. doi:10.1016/j.colsurfa.2020.124761

40. Atsamnia D, Hamadache M, Hanini S, Benkortbi O, Oukrif D. Prediction of the antibacterial activity of garlic extract on E. coli, S. aureus and B. subtilis by determining the diameter of the inhibition zones using artificial neural networks. *LWT Food Sci Technol*. 2017;82:287–295. doi:10.1016/j.lwt.2017.04.053

41. Díaz-García D, Ardiles PR, Díaz-Sánchez M, et al. Copper-functionalized nanostructured silica-based systems: study of the antimicrobial applications and ROS generation against gram positive and gram negative bacteria. *J Inorg Biochem*. 2020;203:110912. doi:10.1016/j.jinorgbio.2019.110912

42. Tang Z, Liu S, Chen N, Luo M, Wu J, Zheng Y. Gold nanoclusters treat intracellular bacterial infections: eliminating phagocytic pathogens and regulating cellular immune response. *Colloids Surf B*. 2021;205:111899. doi:10.1016/j.colsurfb.2021.111899

43. Ashrafizadeh SN, Motaee E, Hoshyargar V. Emulsification of heavy crude oil in water by natural surfactants. *J Petroleum Sci Eng*. 2012;86-87:137–143. doi:10.1016/j.petrol.2012.03.026

44. Almeida F, Corrêa M, Zaera AM, Garrigues T, Isaac V. Influence of different surfactants on development of nanoemulsion containing fixed oil from an amazon palm species. *Colloids Surf A*. 2022;643:128721. doi:10.1016/j.colsurfa.2022.128721

45. Sosa L, Clares B, Alvarado HL, Bozal N, Domenech O, Calpena AC. Amphotericin B releasing topical nanoemulsion for the treatment of candidiasis and aspergillosis. *Nanomed Nanotechnol Biol Med*. 2017;13(7):2303–2312. doi:10.1016/j.nano.2017.06.021

46. Samiun WS, Ashari SE, Salim N, Ahmad S. Optimization of processing parameters of nanoemulsion containing aripiprazole using response surface methodology. *Int j Nanomed*. 2020;15:1585–1594. doi:10.2147/IJN.S198914

47. Jan Y, Al-Keridis LA, Malik M, et al. Preparation, modelling, characterization and release profile of vitamin D3 nanoemulsion. *LWT*. 2022;169:113980. doi:10.1016/j.lwt.2022.113980

48. Liew SN, Utra U, Alias AK, Tan TB, Tan CP, Yussof NS. Physical, morphological and antibacterial properties of lime essential oil nanoemulsions prepared via spontaneous emulsification method. *LWT*. 2020;128:109388. doi:10.1016/j.lwt.2020.109388

49. Feng J, Shi Y, Yu Q, Sun C, Yang G. Effect of emulsifying process on stability of pesticide nanoemulsions. *Colloids Surf A*. 2016;497:286–292. doi:10.1016/j.colsurfa.2016.03.024

50. Akram S, Anton N, Omran Z, Vandamme T. Water-in-oil nano-emulsions prepared by spontaneous emulsification: new insights on the formulation process. *Pharmaceutics*. 2021;13(7):1. doi:10.3390/pharmaceutics13071030

51. Souto EB, Cano A, Martins-Gomes C, Coutinho TE, Zielińska A, Silva AM. Microemulsions and nanoemulsions in skin drug delivery. bioengineering. *Basel Switzerland*. 2022;9(4). doi:10.3390/bioengineering9040158

52. Yu-chen ZHOU, Jia-huan CHEN. Chemical constituents from Zanthoxylum avicennae and their antibacterial activities. *Chinese Traditional Patent Med*. 2023;1:1–5.

53. Yeung AWK, Heinrich M, Atanasov AG. Ethnopharmacology—A bibliometric analysis of a field of research meandering between medicine and food science? *Front Pharmacol*. 2018. doi:10.3389/fphar.2018.00215

54. Ilić K, Hartl S, Galić E, et al. Interaction of differently coated silver nanoparticles with skin and oral mucosal cells. *J Pharmaceut Sci*. 2021;110 (5):2250–2261. doi:10.1016/j.xphs.2021.01.030

55. Zhao X, Wang Y, Zhu TT, et al. Mesoporous calcium-silicate nanoparticles loaded with Prussian blue promotes enterococcus faecalis ferroptosis-like death by regulating bacterial redox pathway ROS/GSH. *Int j Nanomed*. 2022;17:5187–5205. doi:10.2147/IJN.S382928

56. Aslam H, Bi S, Irshadullah M. Analysis of antioxidant enzymes and oxidative stress markers in the liver of naturally infected Indian water buffalo (Bubalus bubalis) with cystic echinococcosis. *J Parasitic Dis*. 2023;47(2):340–348. doi:10.1007/s12639-023-01578-7

57. Pei S, Liu R, Gao H, et al. Inhibitory effect and possible mechanism of carvacrol against Colletotrichum fructicola. *Postharvest Biol Technol*. 2020;163:111126. doi:10.1016/j.postharvbio.2020.111126

58. Rodrigues M, Kosaric N, Bonham CA, Gurtner GC. Wound Healing: a Cellular Perspective. *Physiol Rev*. 2018;99(1):665–706. doi:10.1152/physrev.00067.2017

59. Rousselle P, Braye F, Dayan G. Re-epithelialization of adult skin wounds: cellular mechanisms and therapeutic strategies. *Adv Drug Delivery Rev*. 2019;146:344–365. doi:10.1016/j.addr.2018.06.019

60. Shamilov R, Ackley TW, Aneskievich BJ. Enhanced wound healing- and inflammasome-associated gene expression in TNFAIP3-interacting protein 1- (TNIP1-) deficient HaCaT keratinocytes parallels reduced reepithelialization. *Mediators Inflammation*. 2020;2020:5919150. doi:10.1155/2020/5919150

61. Zhang F, Liu Y, Wang S, et al. Interleukin-25-mediated-IL-17RB upregulation promotes cutaneous wound healing in diabetic mice by improving endothelial cell functions. *Front Immunol*. 2022. doi:10.3389/fimmu.2022.809755

62. Nazıroğlu M. A novel antagonist of TRPM2 and TRPV4 channels: carvacrol. *Metabolic Brain Disease*. 2022;37(3):711–728. doi:10.1007/s11011-021-00887-1

63. Huang K, Liu W, Wei W, et al. Photothermal hydrogel encapsulating intelligently bacteria-capturing bio-MOF for infectious wound healing. *ACS Nano*. 2022;16(11):19491–19508. doi:10.1021/acsnano.2c09593

64. Yates C, May K, Hale T, et al. Wound chronicity, inpatient care, and chronic kidney disease predispose to mrsa infection in diabetic foot ulcers. *Diabetes Care*. 2009;32(10):1907–1909. doi:10.2337/dc09-0295

65. de Souza ML, Oliveira DD, Pereira NDP, Soares DM. Nanoemulsions and dermatological diseases: contributions and therapeutic advances. *Int J Dermatol*. 2018;57(8):894–900. doi:10.1111/ijd.14028

Dovepress